EIT imaging with the projection filter

Bong-Seok Kim*, Min-Chan Kim**, Sin Kim***, and Kyung-Youn Kim*

* Department of Electrical and Electronic Engineering, Cheju National University, Cheju, Korea
(Tel : +82-64-754-3664; E-mail: kyungyk@cheju.ac.kr)
** Department of Chemical Engineering, Cheju National University, Cheju, Korea
(Tel : +82-64-754-3685; E-mail: mckim@cheju.ac.kr)
*** Department of Nuclear and Energy Engineering, Cheju National University, Cheju, Korea
(Tel : +82-64-754-3647; E-mail: sinkim@cheju.ac.kr)

Abstract: Electrical impedance tomography(EIT) is a relatively new imaging modality in which the internal impedivity distribution is reconstructed based on the known sets of injected currents and measured voltages on the surface of the object. In this paper, an effective dynamic EIT imaging scheme is presented based on the projection filtering to estimate the unknown resistivity distribution. In particular, pre-integration (pre-grouping) technique is employed to stabilize the inverse algorithm. We carried out computer simulations with synthetic data to illustrate the reconstruction performance of the proposed algorithm.

Keywords: electrical impedance tomography, extended Kalman filter, projection filter, inverse problem, grouping

1. INTRODUCTION

Over the past few decades, Electrical Tomography (ET) techniques have received much attention in both theoretical and practical points of view since they can be used as an alternative imaging modality in many fields of engineering. This is mainly due to the relatively low-cost requirements, noninvasive measurement sensing, and relatively good temporal resolution [1], [2].

In Electrical Impedance Tomography (EIT), the quantity to be imaged is actually the impedivity distribution inside an object. More frequently in EIT, however, it is assumed that the resistive part of the impedivity distribution is dominated and hence, only the resistivity distribution is estimated and reconstructed as images. In EIT, an array of disjoint electrodes is attached on the boundary of an object and a set (frame) of small alternating currents is injected into the object through these electrodes, and then the corresponding set of voltages is measured on the same array of the electrodes. The objective in EIT is to estimate and reconstruct the resistivity distribution inside the object as soon and as accurately as possible based on the set of measured voltages and injected currents. Image reconstruction in EIT is a kind of highly nonlinear and ill-posed optimization problem which is composed of the forward and inverse problems.

The forward problem in which electrical potential is obtained with the known resistivity distribution is governed by a partial differential equation with appropriate boundary conditions. Owing to the complexity of the forward problem, it is in almost cases impossible to obtain an analytical solution so that the numerical technique such as the finite element method (FEM) is often employed. The EIT inverse problem in which the unknown resistivity distribution is estimated from the potential measured on the boundary of the object is a nonlinear ill-posed problem. Many different approaches to the EIT inverse problem with various regularization methods have been proposed in many literatures [3], [4].

Most of the reconstruction algorithms presented so far have been mainly focused on the case where the internal resistivity distribution of the object is time-invariant within the time taken to acquire a full set of independent measurement data. As is well known, the conventional EIT imaging techniques such as a backprojection (BP) or modified Newton-Raphson (mNR) algorithm [3] use a full set of voltage measurements for one image. However, these techniques often fail to obtain satisfactory temporal resolution for the reconstructed images in case the resistivity distribution inside the object changes rapidly in time.

More recently, dynamic imaging techniques have been developed to enhance the temporal resolution of the reconstructed images in the situations where the resistivity distribution changes rapidly in time. In most of these techniques, the inverse problem is treated as a nonlinear stochastic state estimation problem, and the time-varying state (resistivity) is estimated on-line with the aid of the nonlinear Kalman filter such as the linearized Kalman filter (LKF) [4], [5] and extended Kalman filter (EKF) [6], [7].

In this paper, we developed an effective dynamic EIT reconstruction scheme based on the projection filtering (PF) algorithm [10]. In the projection filter, the filter gain does not depend on the error covariance matrix and leads to fast convergence to optimal estimation. In particular, pre-integration (pre-grouping) technique is employed to stabilize the inverse algorithm. Through the extensive simulations, it is shown that the proposed scheme is more effective than the existing dynamic methods in terms of the spatial and temporal resolutions.

2. FORMULATION OF THE FORWARD PROBLEM

The forward problem is to compute the electrical potential when the injected current and the resistivity distribution are given. When electrical currents, $I_l(l = 1, 2, \ldots, L)$ are injected into the object $\Omega \in \Re^2$ through the electrodes, $e_l(l = 1, 2, \ldots, L)$ attached on the boundary $\partial\Omega$ and the resistivity distribution $\rho(x, y)$ is known for the Ω, the corre-

sponding electrical potential $u(x, y)$ on the Ω can be determined uniquely from the following partial differential equation, which can be derived from the Maxwell equations:

$$\nabla \cdot (\rho^{-1} \nabla u) = 0 \quad \text{in } \Omega. \tag{1}$$

The boundary conditions in the complete electrode model (CEM) [8] are given as:

$$u + z_l \rho^{-1} \frac{\partial u}{\partial n} = U_l \quad \text{on } e_l, \quad l = 1, 2, \ldots, L \tag{2}$$

$$\int_{e_l} \rho^{-1} \frac{\partial u}{\partial n} ds = I_l, \quad l = 1, 2, \ldots, L \tag{3}$$

$$\rho^{-1} \frac{\partial u}{\partial n} = 0 \quad \text{on } \partial\Omega \Big\backslash \bigcup_{l=1}^{L} e_l \tag{4}$$

where z_l is the effective contact impedance between the l-th electrode and the electrolyte, U_l is the potential on the l-th electrode, e_l is the l-th electrode, n is the outward unit normal, and L is the number of electrodes. The boundary conditions, Eqs. (2)$\sim$(4) take into account the shunting effect (i.e., the voltage U_l is constant over the electrode e_l) and the additional voltage drop due to the contact impedance.
In addition, the following two conditions for the injected currents and measured voltages are needed to ensure the existence and uniqueness of the solution [9]:

$$\sum_{l=1}^{L} I_l = 0 \tag{5}$$

$$\sum_{l=1}^{L} U_l = 0. \tag{6}$$

In general, the forward problem cannot be solved analytically, we have to resort to the numerical method. In this paper, we used the finite element method (FEM) to obtain the numerical solution. In the FEM, the object area is discretized into sufficiently small elements having a node at each corner, and it is assumed that the resistivity distribution is constant within each element. The potential at each node and the "referenced" electrode voltages, defined by the vector $v \in \Re^{(M+L-1)\times 1}$, are calculated by discretizing Eq. (1) into $\mathbf{Y}v = c$, where $\mathbf{Y} \in \Re^{(M+L-1)\times(M+L-1)}$ is the so-called stiffness matrix and M is the number of FEM nodes. $\mathbf{Y}$ and c are the functions of the resistivity distribution inside the object and the injected currents through the electrodes, respectively. For more details on the forward solution and the FEM approach, see [4].

3. THE DYNAMIC MODEL AND THE INVERSE PROBLEM

3.1. Parameterization of the state

Sometimes in real applications, there are known internal structures. The FEM elements in each known structure can be grouped together before inverse procedure to stabilize the solution. By pre-grouping we mean that some part of the elements are grouped together and considered as one element before the reconstruction so that the number of states to be estimated is reduced. The pre-grouping can be written in the form

$$\tilde{\rho} \equiv \mathbf{G}\rho \tag{7}$$

where, $\rho \in \Re^{N_f \times 1}$ is the resistivities of the elements in the forward mesh, $\tilde{\rho} \in \Re^{N_g \times 1}$ is the resistivities of the grouped elements, N_f and N_g is the number of forward elements and grouped elements in the finite element mesh,respectively, and $\mathbf{G} \in \Re^{N_g \times N_f}$ is the sparse grouping matrix that includes inverse of the number of the elements to be grouped in the specific locations such that it maps the resistivities in ρ to the correct element locations in $\tilde{\rho}$. The FEM meshes used in the forward and grouped inverse meshes are shown in Fig. 1.

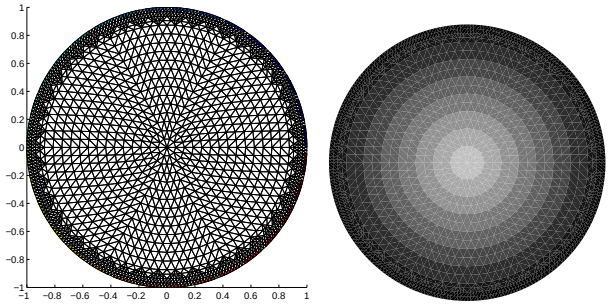

(a) (b)

Fig. 1. The FEM mesh used for (a) forward solver with 3104 elements and (b) inverse solver with 9 pre-grouped regions.

3.2. Dynamic model

We consider the underlying inverse problem as a stochastic state estimation problem to estimate time-varying distribution of the resistivity on-line. In the state estimation problem, we need the dynamic model which consists of the state equation for the temporal evolution of the resistivity distribution and the measurement equation for the relationship between the resistivity distribution and boundary voltage. In general, the temporal evolution of the resistivity distribution $\tilde{\rho}_k$ in the object Ω is related by the nonlinear mapping. Here, the state equation is assumed to be of the linear form, of which the modeling uncertainty is compensated by the process noise:

$$\tilde{\rho}_{k+1} = \mathbf{F}_k \tilde{\rho}_k + w_k \tag{8}$$

where $\tilde{\rho}_k \in \Re^{N_g \times 1}$ is the state vector (resistivity distribution) at time k, $\mathbf{F}_k \in \Re^{N_g \times N_g}$ is the state transition matrix. In particular, we take $\mathbf{F}_k = \mathbf{I}_{N_g}$ for all k, where $\mathbf{I}_{N_g} \in \Re^{N_g \times N_g}$ is the identity matrix, to obtain the so-called random-walk model. It is assumed that the process noise, w_k is the white Gaussian noise with the following covariance matrix which determines the rate of changes in resistivity distribution

$$\Gamma_k^w = E[w_k w_k^T] \in \Re^{N_g \times N_g}. \tag{9}$$

Let the measurement vector, $U_k \in \Re^{L \times 1}$ defined as

$$U_k \equiv [U_k^1, U_k^2, \ldots, U_k^L]^T \tag{10}$$

be the surface measurement voltages induced by the k-th current pattern on the electrodes. And then the measurement equation can be described as the following nonlinear mapping with the measurement noise

$$U_k = V_k(\tilde{\rho}_k) + v_k \tag{11}$$

where the measurement noise v_k is assumed to be the white Gaussian noise with the covariance matrix as

$$\Gamma_k^v = E[v_k v_k^T] \in \Re^{L\times L}. \tag{12}$$

Linearizing Eq. (11) about the current predicted state vector $\hat{\rho}_{k|k-1}$ we obtain

$$U_k = V_k(\hat{\rho}_{k|k-1}) + \mathbf{J}_k(\hat{\rho}_{k|k-1})(\tilde{\rho}_k - \hat{\rho}_{k|k-1}) + H.O.Ts + v_k \tag{13}$$

where $H.O.Ts$ represents the higher-order terms which will be considered as additional noise, and $\mathbf{J}_k(\hat{\rho}_{k|k-1}) \in \Re^{L\times N_g}$ is the Jacobian matrix defined by

$$\mathbf{J}_k(\hat{\rho}_{k|k-1}) \equiv \left.\frac{\partial V_k}{\partial \tilde{\rho}}\right|_{\tilde{\rho}=\hat{\rho}_{k|k-1}}. \tag{14}$$

Let us define the pseudo-measurement vector as

$$y_k \equiv U_k - V_k(\hat{\rho}_{k|k-1}) + \mathbf{J}_k(\hat{\rho}_{k|k-1})\hat{\rho}_{k|k-1}. \tag{15}$$

Then we obtain the linearized measurement equation by considering the $H.O.Ts$ in Eq. (13) as additional noise

$$y_k = \mathbf{J}_k(\hat{\rho}_{k|k-1})\tilde{\rho}_k + \nu_k \tag{16}$$

where ν_k is composed of the measurement noise and linearization error, and also assumed to be the white Gaussian noise with the covariance matrix as

$$\Gamma_k^\nu = E[\nu_k \nu_k^T] \in \Re^{L\times L}. \tag{17}$$

In filtering algorithm we estimate the state vector $\tilde{\rho}_k$ based on all the measurements taken up to the time k. With the Gaussian assumptions the required estimate is obtained by minimizing the cost functional which is formulated based on the above state and measurement equations, Eqs. (8) and (16), respectively. The cost functional is of the form

$$\begin{aligned}\Xi(\tilde{\rho}_k) = \tfrac{1}{2}\Big\{ &\left\|\tilde{\rho}_k - \hat{\rho}_{k|k-1}\right\|^2_{\mathbf{C}^{-1}_{k|k-1}} \\ &+ \left\|y_k - \mathbf{J}_k(\hat{\rho}_{k|k-1})\tilde{\rho}_k\right\|^2_{(\Gamma_k^\nu)^{-1}}\Big\}\end{aligned} \tag{18}$$

where $\mathbf{C}_{k|k-1} \in \Re^{N_g\times N_g}$ is the time-updated error covariance matrix, which is defined by

$$\mathbf{C}_{k|k-1} \equiv E[(\tilde{\rho}_k - \hat{\rho}_{k|k-1})(\tilde{\rho}_k - \hat{\rho}_{k|k-1})^T]. \tag{19}$$

3.3. Regularization method

In order to mitigate the inherent ill-posed nature of the EIT inverse problem, additional constraint is included in the cost functional

$$\begin{aligned}\Xi(\rho_k) = \tfrac{1}{2}\Big\{ &\left\|\tilde{\rho}_k - \hat{\rho}_{k|k-1}\right\|^2_{\mathbf{C}^{-1}_{k|k-1}} \\ &+ \left\|y_k - \mathbf{J}_k(\hat{\rho}_{k|k-1})\tilde{\rho}_k\right\|^2_{(\Gamma_k^\nu)^{-1}} + \alpha\left\|\mathbf{R}\tilde{\rho}_k\right\|^2\Big\}\end{aligned} \tag{20}$$

where α is the regularization parameter which is chosen empirically, and $\mathbf{R} \in \Re^{N_g\times N_g}$ is the generalized Tikhonov regularization matrix [4] with the smoothness assumptions on the resistivity distribution. In this paper, the resistivity distribution is parameterized such that

$$\tilde{\rho} = \sum_{n=1}^{N_g} \tilde{\rho}_n \chi_n \tag{21}$$

where χ_n is the characteristic function of the n-th finite element. The i-th row of matrix $\mathbf{R}$ is

$$\mathbf{R}_i = (0, \ldots, -1, 0, \ldots, 2, 0, \ldots, -1, 0, \ldots, 0) \tag{22}$$

where 2 is located at the i-th column and -1 is placed in the columns corresponding to elements having common edge with the i-th element. This is the reason why the i-th element is located in the grouped region has two edges.

For the computations, if we define the augmented pseudo-measurement vector, $\tilde{y}_k \in \Re^{(L+N_g)\times 1}$ and the pseudo-measurement matrix, $\mathbf{H}_k \in \Re^{(L+N_g)\times N_g}$ as

$$\tilde{y}_k \equiv \begin{pmatrix} y_k \\ 0 \end{pmatrix} \tag{23}$$

$$\mathbf{H}_k \equiv \begin{pmatrix} \mathbf{J}_k(\hat{\rho}_{k|k-1}) \\ \sqrt{\alpha}\mathbf{R} \end{pmatrix} \tag{24}$$

then the cost functional, Eq. (20) can be rearranged as

$$\Xi(\tilde{\rho}_k) = \frac{1}{2}\left\{\left\|\tilde{\rho}_k - \hat{\rho}_{k|k-1}\right\|^2_{\mathbf{C}^{-1}_{k|k-1}} + \left\|\tilde{y}_k - \mathbf{H}_k\tilde{\rho}_k\right\|^2_{\Gamma_k^{-1}}\right\} \tag{25}$$

where the augmented covariance matrix of the noise, $\Gamma_k \in \Re^{(L+N_g)\times(L+N_g)}$ is defined by

$$\Gamma_k \equiv Blockdiag\left[\Gamma_k^\nu, \mathbf{I}_{N_g}\right]. \tag{26}$$

3.4. Extended Kalman filter

By minimizing the cost functional, Eq. (25) and solving for the updates of the associated covariance matrices, we obtain the recursive extended Kalman filter (EKF) [6] which consists of the following two procedures:

(i) *Measurement updating step* (*filtering*)

$$\mathbf{K}_k = \mathbf{C}_{k|k-1}\mathbf{H}_k^T\left(\mathbf{H}_k\mathbf{C}_{k|k-1}\mathbf{H}_k^T + \Gamma_k\right)^{-1} \tag{27}$$

$$\mathbf{C}_{k|k} = \left(\mathbf{I} - \mathbf{K}_k\mathbf{H}_k\right)\mathbf{C}_{k|k-1} \tag{28}$$

$$\hat{\rho}_{k|k} = \hat{\rho}_{k|k-1} + \mathbf{K}_k\left(\tilde{y}_k - \mathbf{H}_k\hat{\rho}_{k|k-1}\right) \tag{29}$$

(ii) *Time updating step* (*prediction*)

$$\mathbf{C}_{k+1|k} = \mathbf{F}_k\mathbf{C}_{k|k}\mathbf{F}_k^T + \Gamma_k^w \tag{30}$$

$$\hat{\rho}_{k+1|k} = \mathbf{F}_k\hat{\rho}_{k|k} \tag{31}$$

where $\mathbf{K}_k$ is the Kalman gain matrix at time k, $\hat{\rho}_{k|k}$ is the estimate of the true state vector $\tilde{\rho}_k$ in a recursive minimum mean square error sense for $k = 1, 2, \ldots, rp$, where p is the number of the independent current patterns and r is the number of the classical frames.

3.5. Projection filter

In this subsection, by minimizing the cost functional, Eq. (25), we wish to apply a new filtering algorithm based on the projection filter [10], instead of the above Kalman filter algorithm to estimate the resistivity distribution. This algorithm can be given as the following sequences:

(i) *Measurement updating step* (*filtering*)

$$\mathbf{K}_k = \left(\mathbf{H}_k^T \Gamma_k^{-1} \mathbf{H}_k\right)^{-1} \mathbf{H}_k^T \Gamma_k^{-1} \tag{32}$$

$$\begin{aligned}\mathbf{C}_{k|k} = \mathbf{C}_{k|k-1} + \mathbf{K}_k \left(\mathbf{H}_k \mathbf{C}_{k|k-1} \mathbf{H}_k^T + \Gamma_k\right) \mathbf{K}_k^T \\ -\mathbf{K}_k \mathbf{H}_k \mathbf{C}_{k|k-1} - \mathbf{C}_{k|k-1} \mathbf{H}_k^T \mathbf{K}_k^T\end{aligned} \tag{33}$$

$$\hat{\rho}_{k|k} = \hat{\rho}_{k|k-1} + \mathbf{K}_k \left(\tilde{y}_k - \mathbf{H}_k \hat{\rho}_{k|k-1}\right) \tag{34}$$

(ii) *Time updating step* (*prediction*)

$$\mathbf{C}_{k+1|k} = \mathbf{F}_k \mathbf{C}_{k|k} \mathbf{F}_k^T + \Gamma_k^w \tag{35}$$

$$\hat{\rho}_{k+1|k} = \mathbf{F}_k \hat{\rho}_{k|k} \tag{36}$$

In the new filtering algorithm, it is obvious that the filter gain matrix, Eq. (32) does not depend on the error covariance matrix, $\mathbf{C}_{k|k-1}$ in contrast with the Kalman gain matrix, Eq. (27). This very important feature leads to fast convergence to the optimal estimate of the true state.

4. COMPUTER SIMULATIONS

We carried out extensive computer simulations with synthetic data to evaluate the reconstruction performance of the proposed algorithm. In this simulations, the complete electrode model with the contact impedance of $0.005\Omega cm$ is employed. The finite element meshes used for the forward and inverse solvers are shown in Fig. 1(a) and 1(b), respectively. In the forward computations we used the FEM with a mesh of 3104 elements (N_f) and 1681 nodes (M). The elements in the FEM mesh are pre-grouped into 9 regions (N_g) in the inverse computations. Adjacent current patterns [1] were injected into the object Ω with $1cm$ in diameter through 32 electrodes ($L = 32$) for 1 classical frame.

The reconstruction performance of the proposed scheme is compared with those of the mNR and the EKF for the static and dynamic situations. Here, 'static' and 'dynamic' mean that the resistivity distribution inside the object change and does not change within 1 classical frame, respectively.

It is assumed that the covariance matrices used for the EKF and PF are diagonal and time-invariant. To clarify the estimation performance of the EKF and PF algorithms, we calculate the relative root-mean-square error (RMSE) for each current pattern k defined by

$$RMSE(k) \equiv \sqrt{\frac{(\tilde{\rho}_k - \hat{\rho}_{k|k})^T (\tilde{\rho}_k - \hat{\rho}_{k|k})}{\tilde{\rho}_k^T \tilde{\rho}_k}} \tag{37}$$

4.1. Static image reconstruction

In this static simulation, it is assumed that the covariance matrix for the process noise (Γ_k^w) is $0\mathbf{I}_{N_g}$, the covariance matrix for the measurement noise (Γ_k^ν) is $10^{-4}\mathbf{I}_{N_g}$, and the initial value for the error covariance matrix ($\mathbf{C}_{1|0}$) is set to the identity matrix, $\mathbf{I}_{N_g}$.

Fig. 2 shows images reconstructed by three methods according to the regularization parameter α, that is, the first row is $\alpha = 0.00001$, the second row is $\alpha = 0.001$, the third row is $\alpha = 0.1$, the forth row is $\alpha = 10$.

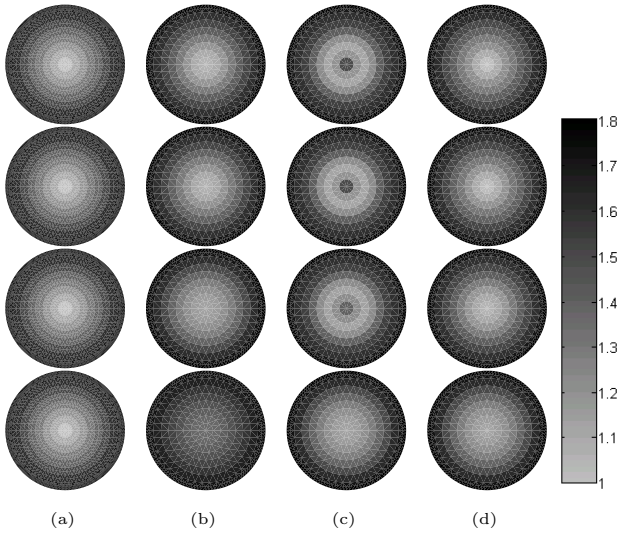

Fig. 2. Reconstructed images for the static situation with different α. (a) true images, (b) images reconstructed by the mNR, (c) images reconstructed by the EKF, and (d) images reconstructed by the PF.

As can be seen from Fig. 2, images reconstructed by the projection filter are more similar to the true images than those reconstructed by other methods in selected α values. The reconstruction performance of the mNR is deteriorated for larger α values while that of the EKF is deteriorated for smaller α values. It is noted that the projection filter reveals good reconstruction performance for the static situation in a wide range of α values.

To clarify the estimation performance of the proposed algorithm, we calculate the relative root-mean-square error (RMSE) defined by Eq. (37). Fig. 3 shows the RMSEs between the true and estimated resistivities according to the regularization parameter α (the bold line is $\alpha = 0.00001$, the bold dotted line is $\alpha = 0.001$, the thin line is $\alpha = 0.1$, and the thin dotted line is $\alpha = 10$). As can be seen clearly, the reconstruction performance of the projection filter is enhanced than those of other methods with less computational burden. Note that the abscissa of Fig. 3(a) represents the off-line iteration number while those of Fig. 3(b) and 3(c) represent on-line measurement instants.

4.2. Dynamic image reconstruction

To simulate the dynamic situation, the true images are changed abruptly three times for 1 classical frame as shown in the first columns in Figs. 4∼6. In this dynamic simulation, it is assumed that the covariance matrix for the process noise (Γ_k^w) is $10\mathbf{I}_{N_g}$, the covariance matrix for the measurement noise (Γ_k^ν) is $10^{-4}\mathbf{I}_{N_g}$, and the initial value for the error covariance matrix ($\mathbf{C}_{1|0}$) for the estimate is set to the identity matrix, $\mathbf{I}_{N_g}$.

Figs. 4∼6 show images reconstructed by three methods with different regularization parameter α (Fig. 4 is for

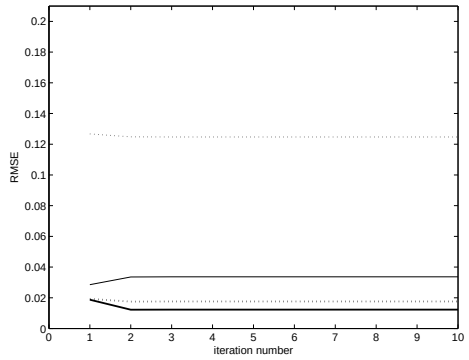

(a)

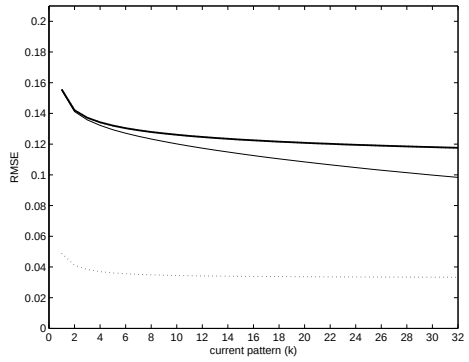

(b)

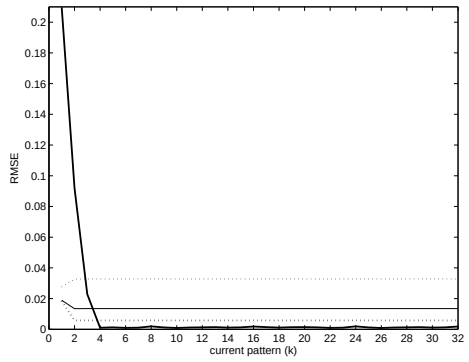

(c)

Fig. 3. RMSEs between the true and estimated resistivities for the static situation. (a) RMSE for the mNR, (b) RMSE for the EKF, and (c) RMSE for the PF.

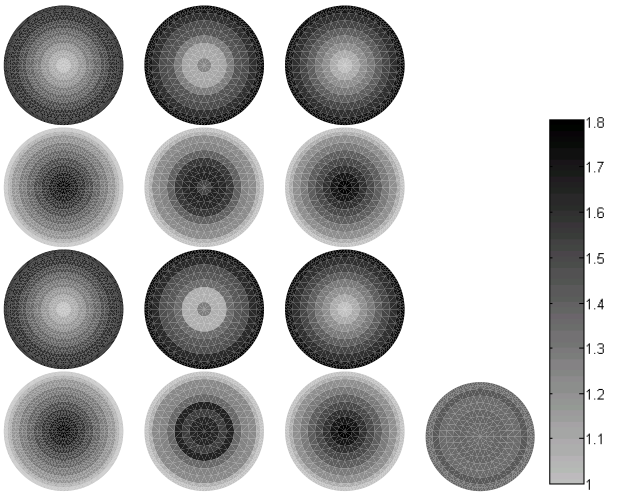

(a) (b) (c) (d)

Fig. 4. Reconstructed images for the dynamic situation with $\alpha = 0.0001$. (a) true images, (b) images reconstructed by the EKF, (c) images reconstructed by the PF, and (d) images reconstructed by the mNR.

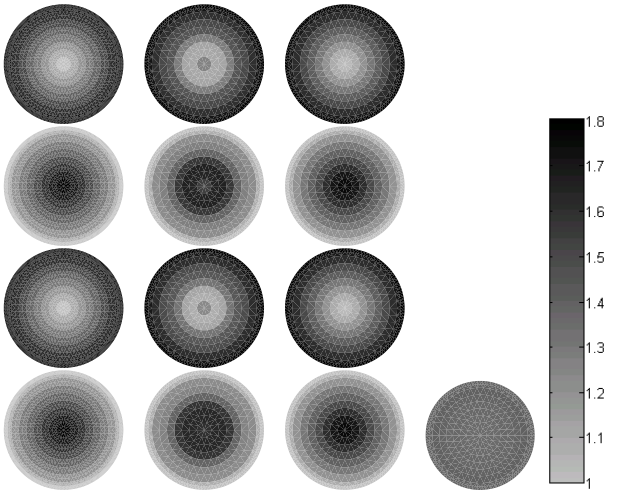

(a) (b) (c) (d)

Fig. 5. Reconstructed images for the dynamic situation with $\alpha = 0.01$. (a) true images, (b) images reconstructed by the EKF, (c) images reconstructed by the PF, and (d) images reconstructed by the mNR.

$\alpha = 0.0001$, Fig. 5 is for $\alpha = 0.01$, and Fig. 6 is for $\alpha = 1$).

As can be seen from these figures, images reconstructed by the projection filter are enhanced than those reconstructed by other methods. Similar to the static case, the reconstruction performance of the EKF is deteriorated for weak regularizations. As can be expected, the temporal information is lost in the reconstructed images by the mNR.

In addition, we calculate the RMSE to clarify the estimation performance of the proposed algorithm. Fig. 7 shows the RMSEs between the true and estimated resistivities with different regularization parameter α (the bold line is $\alpha = 0.0001$, the bold dotted line is $\alpha = 0.01$, and the thin line is $\alpha = 1$). As can be seen clearly, the estimation performance of the projection filter is better than that of the EKF in the dynamic situation.

5. CONCLUSIONS

Quite often in real situations, the resistivity distribution inside the object changes rapidly within measurement of 1 classical frame.

In this paper, we propose a dynamic EIT reconstruction scheme based on the projection filter. In particular, pre-integration (pre-grouping) technique is employed to stabilize the inverse algorithm. We formulated the EIT inverse problem as a stochastic state estimation problem and the state (resistivity distribution) is estimated on-line with the aid of the projection filter. Through the extensive computer simulations, it is shown that the proposed reconstruction algorithm reveals enhanced reconstruction performance for both static and dynamic situations.

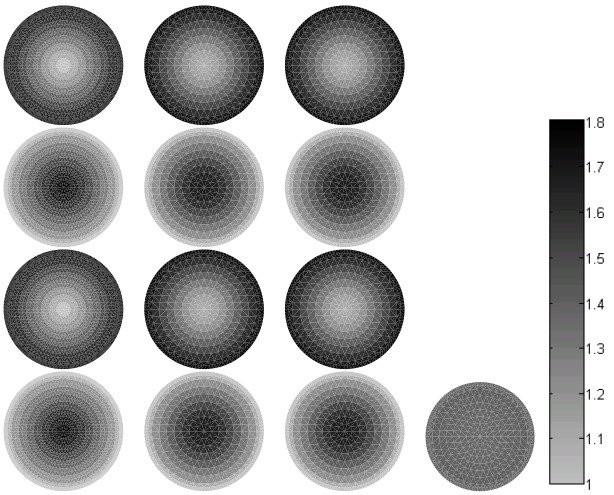

Fig. 6. Reconstructed images from the dynamic situation with $\alpha = 1$. (a) true images, (b) images reconstructed by the EKF, (c) images reconstructed by the PF, and (d) images reconstructed by the mNR.

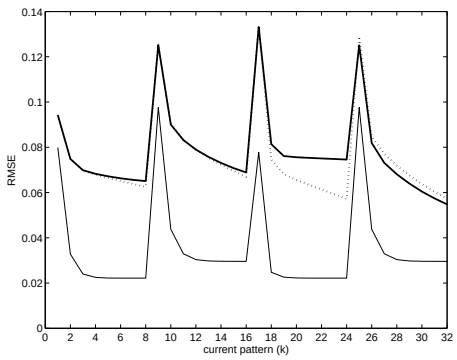

(a)

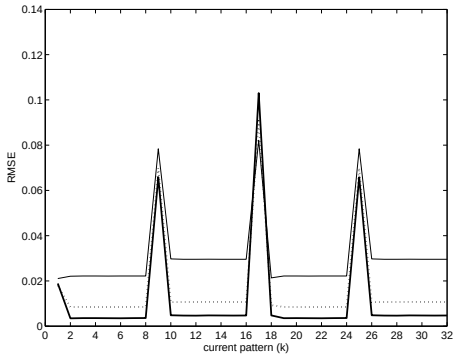

(b)

Fig. 7. RMSEs between the true and the estimated resistivities for the dynamic situation. (a) RMSE for the EKF and (b) RMSE for the PF.

ACKNOWLEDGEMENTS

This work was supported by grant No. R01-2002-000-0040-0 (2002) from the Basic Research Program of the Korea Science and Engineering Foundation.

References

[1] J.G. Webster, *Electrical Impedance Tomography*, Adam Hilger, 1990.

[2] R.A. Williams and M.S. Beck, *Process Tomography : Principles, Techniques and Applications*, Butterworth-Heinemann, Oxford, 1995.

[3] T.J. Yorkey, J.G. Webster, and W.J. Tompkins, "Comparing reconstruction algorithms for electrical impedance tomography," *IEEE Transactions on Biomedical Engineering*, Vol. 34, No. 11, pp. 843-852, 1987.

[4] M. Vauhkonen, *Electrical Impedance Tomography and Prior Information*, Doctoral Dissertation, Dept. of Applied Physics, University of Kuopio, Finland, 1997.

[5] M. Vauhkonen, P.A. Karjalainen, and J.P. Kaipio, "A Kalman filter approach to track fast impedance changes in electrical impedance tomography," *IEEE Transactions on Biomedical Engineering*, Vol. 45, No. 4, pp. 486-493, 1998.

[6] K.Y. Kim, B.S. Kim, M.C. Kim, Y.J. Lee, and M. Vauhkonen, "Image reconstruction in time-varying electrical impedance tomography based on the extended Kalman filter," *Measurement Science and Technology*, Vol. 12, No. 8, pp. 1032-1039, 2001.

[7] K.Y. Kim, S.I. Kang, M.C. Kim, S. Kim, Y.J. Lee, and M. Vauhkonen, "Dynamic imaging in electrical impedance tomography with known internal structures," *Inverse Problems in Engineering*, Vol. 11, No. 1, pp. 1-19, 2003.

[8] K.S. Cheng, D. Isaacson, J.C. Newell, and D.G. Gisser, "Electrode models for electric current computed tomography," *IEEE Trans. Biomed. Eng.*, Vol. 36, pp. 918-924, 1989.

[9] E. Somersalo, M. Cheney, and D. Isaacson, "Existence and uniqueness for electrode models for electric current computed tomography," *SIAM J. Appl. Math.*, Vol. 52, No. 4, pp. 1023-1040, 1992.

[10] N. Tosaka, A. Utani, and H. Takahashi, "Unknown defect identification in elastic field by boundary element method with filtering procedure," *Engineering Analysis with Boundary Elements*, Elsevier Science Limited, Vol. 15, pp. 207-215, 1995.